Luminescence Study of Polymer Optical Fibers Doped With Conjugated Polymers

Igor Ayesta, María Asunción Illarramendi, Jon Arrue, Felipe Jiménez, Joseba Zubia, Iñaki Bikandi, Jone M. Ugartemendia, and Jose-Ramon Sarasua

***Abstract*—The characterization of the spectral emission and of the photostability of polymer optical fibers (POFs) doped with conjugated polymers has been carried out taking into account the distribution of the dopant in the fiber core. Four different conjugated polymers embedded in the matrix of the typical POF material have been analyzed. Measurements include, among others, evolutions of the emission with excitation wavelength and time, spectral changes for different excitation irradiances, and the influence of the propagation distance along the fiber.**

***Index Terms*—Amplifiers, conjugated polymers, fluorescence, lasers, organic materials, polymer optical fibers.**

I. Introduction

In the last few years, poly(methyl methacrylate) (PMMA) polymer optical fibers (POFs) have raised a great interest in applications such as short-haul communications links, sensing applications and, by using active dopants, also in the field of fiber lasers and amplifiers in the visible region [1]–[5]. POFs have the advantages of being robust, of having large core diameters and high numerical apertures, and of presenting lower manufacturing temperatures as compared to glass fibers. At such temperatures, the core of POFs can be manufactured embedding a wide variety of active materials.

Manuscript received May 18, 2012; revised September 06, 2012; accepted September 06, 2012. Date of publication September 14, 2012; date of current version October 17, 2012. This work was supported by the institutions Ministerio de Ciencia e Innovación, Gobierno Vasco/Eusko Jaurlaritza, and University of the Basque Country (UPV/EHU), under Projects TEC2009-14718-C03-01, AIRHEM-II, SAI12/174, and UFI11/16 respectively. The works of I. Ayesta and J. M. Ugartemendia were supported in part by research fellowships from the University of the Basque Country (UPV/EHU), Vicerrectorado de Euskara y Plurilingüismo, and from the Basque Government (GV/EJ), Department of Education, Universities and Research, respectively, while working on their Ph.D. degree.

I. Ayesta, J. Arrue, J. Zubia, and I. Bikandi are with the Department of Communications Engineering, E.T.S.I. of Bilbao, University of the Basque Country (UPV/EHU), Bilbao 48013, Spain (e-mail: igor.ayesta@ehu.es; jon.arrue@ehu.es; joseba.zubia@ehu.es; inaki.bikandi@ehu.es).

M. A. Illarramendi is with the Department of Applied Physics I, E.T.S.I. of Bilbao, University of the Basque Country (UPV/EHU), Bilbao 48013, Spain (e-mail: ma.illarramendi@ehu.es).

F. Jiménez is with the Department of Applied Mathematics, E.T.S.I. of Bilbao, University of the Basque Country (UPV/EHU), Bilbao 48013, Spain (e-mail: felipe.jimenez@ehu.es).

J. M. Ugartemendia and J. R. Sarasua are with the Department of Mining-Metallurgy and Materials Science, E.T.S.I. of Bilbao, University of the Basque Country (UPV/EHU), Bilbao 48013, Spain (e-mail: jone.munoz@ehu.es; jr.sarasua@ehu.es).

Color versions of one or more of the figures in this paper are available online at http://ieeexplore.ieee.org.

Digital Object Identifier 10.1109/JLT.2012.2218216

Organic dyes and conjugated polymers can be easily embedded in the core of POFs to obtain high gains in particularly short fiber lengths, due to their large absorption and emission cross sections (10 000 times larger than those of Er^{3+} in glass) [6]. Moreover, the conjugated polymers are good candidates for optical switching, due to their fast electronic transitions [5], [7]. Besides, one of the advantages of using conjugated polymers embedded in the solid POF core is the higher photostability that can be obtained as compared to using these dopants embedded in solutions [8]. This is because dopants embedded in solid matrices are partially isolated from impurities that can take part in destructive photochemical reactions [9], and also because the POF cladding improves their photostability, due to the fact that the cladding prevents the reaction of the dopant with oxygen [10]. Besides, the excitation intensity needed to achieve stimulated emissions in optical amplifiers and lasers based on doped fibers is lower than in bulk material, due to the effective confinement and long interaction length available in the fibers. This fact is advantageous because the photostability and the lifetime of the gain medium decrease for higher excitation intensities. On the other hand, note that the photostability in the visible region is reduced if high-energy photons are used (close to the ultraviolet region) to excite dopant molecules [11]. Therefore, efforts are being made to produce new conjugated polymers and oligomers with working wavelength ranges located at longer wavelengths, i.e., in the green-to-red region [12].

Taking into account the aforementioned applications of doped POFs, a thorough characterization of their optical features and of the influence of the host matrix is very useful to improve their performance. Although there are many publications related to the spectroscopic properties of conjugated polymers in many different matrices [5], [13]–[15], little work has been done in POFs. In this paper, we study the optical properties of various conjugated polymers embedded in POFs under side excitation [16], [17] with femtosecond-width laser pulses. On the one hand, excitation with ultrashort pulses allows better understanding of the behavior of doped POFs to develop fast optical devices based on POF technology. On the other hand, side excitation is usually employed for sensing and for light amplification in POFs [18], [19]. Specifically, the emitted spectra as a function of the dopant, the excitation wavelength, and the light propagation distance through the fiber are studied. We also analyze the evolution of the emitted fluorescence characteristics when doped POFs are exposed to laser excitation, in order to gain insight into their photostability properties. Atomic force microscopy (AFM) phase images and transmission electron microscopy (TEM) images have been

taken to analyze the dopant distribution in the matrix. We show that the dopant distribution plays an important role in the optical characteristics of active POFs. The AFM technique is extremely useful for the characterization of heterogeneous materials, such as our doped POFs, which are made of PMMA doped with conjugated polymers. It provides nanometer-scale information about the existence of individual components laid on the surface structure, which enables the detection of some physical properties, as could be viscoelasticity or adhesion. Therefore, these images would be helpful to discern the dopants from the PMMA matrix. Since AFM is only a surface characterization technique, a complementary technique, namely TEM, is also employed. In a TEM microscope, a beam of electrons is transmitted through an ultrathin sample, interacting with the material as it passes through it. Image contrast is produced by the electron scattering of the different components located along the entire thickness. Therefore, TEM allows the identification of the distribution of dopants along a PMMA matrix not only on the surface but also in the entire sample.

This paper is organized as follows. The experimental techniques are described in Section II. In Section III, the spectroscopic properties of the doped POFs are analyzed and discussed. The conclusions are summarized in Section IV.

II. Experiment

Measurements have been carried out using PMMA step-index POFs doped with four different conjugated polymers, namely, poly(9, 9-dioctylfuorene) (PFO), poly(9, 9 dioctylfluorene)-alt-benzothiadiazole (F8BT), poly(9, 9-dioctylfluorene-alt-bithiophene) (F8T2), and poly[2, 7-(9, 9-bis(2'-ethylhexyl)fluorene)-alt-2, 5-terthiophene] (PF3T). In all cases, the dopant concentration in the fiber core is 0.003 wt% and the cladding material is not doped. The fiber diameter is 1 mm, the core diameter being 980 μm, and the cladding thickness being 10 μm. These doped fibers were produced by the POF manufacturer Luceat S.p.A (Italy) using an adapted preform-drawing technique, and their manufacture details are described in [20]. The fiber samples were 30–40 cm long and the fiber ends were carefully polished by hand using polishing papers.

The setup employed to measure the optical spectra can be seen in Fig. 1, in which we can see that the side-illumination technique has been used [16], [17]. The light source used to excite the active fibers was the Mai Tai HP laser system (∼100 fs width laser pulses with peak powers of 300 kW, average power of 2.5 W, repetition rate of 80 MHz) with a frequency doubling unit (Inspire Blue) to be able to excite in the range from 345 to 520 nm. By adjusting manually the variable attenuator placed after the laser output, the impinging irradiance could be controlled.

The measured doped fiber was held between two xy micropositioners standing on a linear stage. These were used to maintain the working area of the fiber totally horizontal and to focus the incident laser beam just on the center of the fiber side. It was not necessary to use a microscope objective in the setup because the laser signal provided by the system was sufficiently collimated to generate a high fluorescence in the doped fiber. In most of

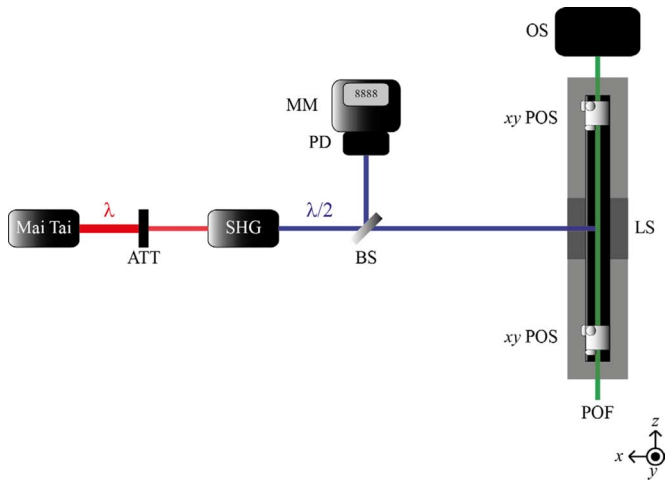

Fig. 1. Experimental setup employed to measure the emission spectra obtained from doped POFs. Legend: ATT: variable Attenuator; SHG: Inspire Blue Second Harmonic Generator; BS: Beam Splitter; PD: Photodetector; MM: Multimeter; LS: Linear Stage; xy POS: xy micropositioner; OS: Optical Spectrometer.

the measurements, the distance from the incidence beam to the output end of the fiber was constant (16 cm). The emission spectrum was also measured as a function of the propagation distance through the doped fiber, by changing the position of the launching point of the light. An ILS250CC linear stage driven by an ESP300 motion controller was used for this purpose. All the emission spectra obtained from the fiber end were measured by a USB4000 fiber-optic spectrometer with an optical resolution of 1.5 nm of full-width at half-maximum (FWHM), and the data obtained were corrected for the response of the detection system. Besides, a reference signal was obtained using a beam splitter to cancel the irradiance fluctuations of the laser. Our own LabVIEW program was built to automate both the motion controller and the spectrometer, and also to achieve a good synchronization during the measurements. The absorption spectra of the doped fibers were obtained from a Cary 50 UV-Vis spectrophotometer equipped with a fiber-optic coupler accessory. In these measurements, the fiber length was short enough (1 cm) to detect the absorption bands of the dyes embedded in the fiber cores.

AFM measurements were carried out with a scanning probe microscope (Nanoscope III Multimode Bruker) equipped with a scanner of maximum range of 100 μm in the xy plane and of 10 μm in the z-direction. Image acquisition was carried out by scanning in tapping mode using a standard silicon cantilever (RTESP Bruker) with a resonance frequency of about 254–321 kHz and a spring constant of about 20–80 Nm^{-1}. Height and phase images were collected simultaneously at a scan rate of 0.5 Hz under ambient conditions. Surfaces of each sample were prepared by microtome sectioning (LEICA EM UC6) and they were cleaned with ethanol prior to measurements. A high-resolution TEM microscope (TECNAI G2 20 TWIN) equipped with a LaB6 filament was used to obtain the images of the four doped fibers. The samples were prepared using the ultramicrotome LEICA EM UC6.

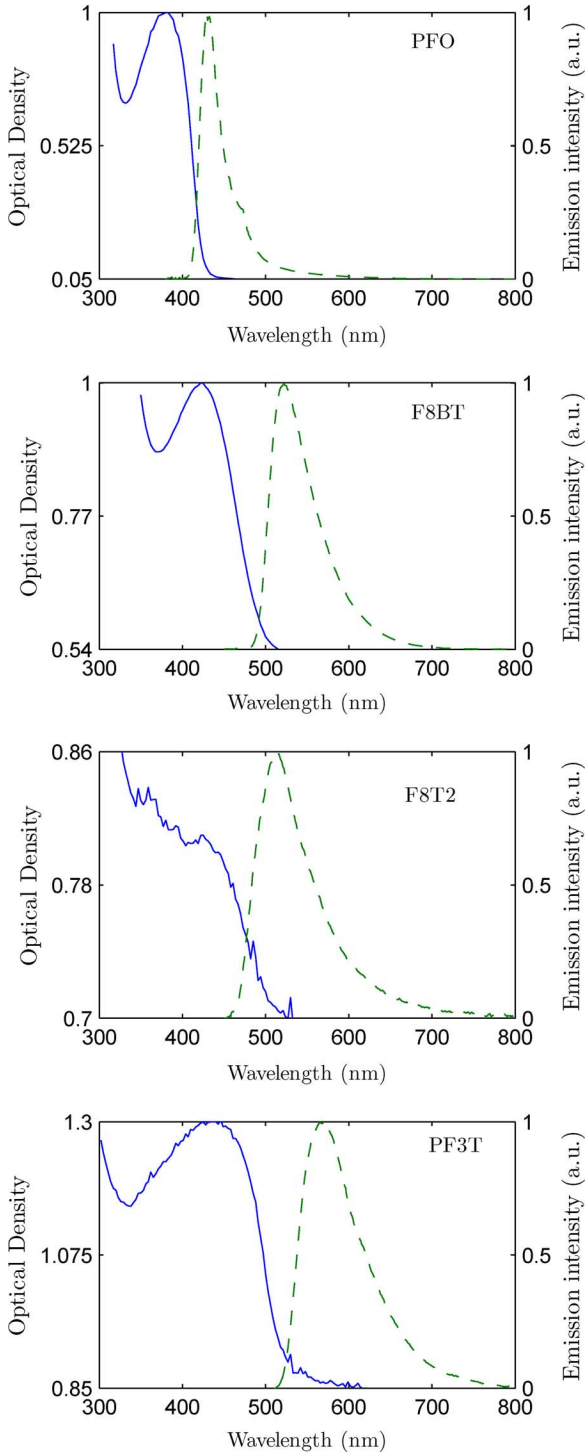

Fig. 2. Absorption (solid lines) and emission (dashed lines) spectra of PFO-, F8BT-, F8T2-, and PF3T-doped POFs. The emission spectra were obtained exciting each sample at its maximum-absorption wavelength with a light propagation distance of 16 cm.

III. Results and Discussion

A. Spectroscopic Analysis

The absorption spectra of the doped fibers in the near-ultraviolet and visible regions are shown in Fig. 2. The maximum-absorption wavelengths obtained are listed in Table I. As can be seen, the fibers doped with F8T2 and PF3T have their maximum absorption at a longer wavelength (440 nm in both cases) than in the other two samples.

TABLE I
Absorption and Emission Characteristics of the Conjugated Polymers Embedded in POFs

Dopant	Absorption peak (nm)	Emission peak (nm)	Emission FWHM(nm)	Stokes shift (nm)	Overlap range (nm)
PFO	380	428	28.7	48	410-425
F8BT	425	522	60.6	97	485-500
F8T2	440	514	76.1	74	460-500
PF3T	440	572	82.7	132	520-600

Fig. 2 also shows the emission spectra for each doped fiber obtained by exciting at the maximum-absorption wavelengths, and the corresponding maximum-emission wavelengths have been added to Table I. It is noticeable that the fibers with PFO and with PF3T present the lowest and the highest emission wavelengths, respectively. The emissions from F8BT- and F8T2-doped fibers are located in the green region of the spectrum, which is a low-attenuation window of PMMA. Table I shows the FWHM of the emission spectra, the Stokes shifts (separations between the maxima of the emission and absorption spectra), and the overlaps between the absorption-emission spectra corresponding to all fibers. It can be noted that PF3T-doped fibers present the highest Stokes shift with the highest overlap. This behavior is explained in terms of a higher vibrational interaction between the matrix and the electrons of the dopant material in the single-configuration coordinate model [21], [22]. As will be shown, the absorption-emission overlap has a direct relationship with the variations of the emission spectra as a function of the light propagation distance along the fiber.

We have measured the emission spectra as a function of the excitation wavelength, with a constant light propagation distance. Since the spectra obtained are not symmetrical, the dependence of the spectral emission properties on the excitation wavelength has been studied by using their first and second moments (N_1 and N_2). The first moment, which represents the average emission wavelength, has been calculated from

$$N_1 = \int I(\lambda)\lambda d\lambda \Big/ \int I(\lambda)d\lambda. \tag{1}$$

The square root of the second moment, which is proportional to the spectral width, is calculated using

$$\sqrt{N_2} = \sqrt{\frac{\int (N_1-\lambda)^2 I(\lambda)d\lambda}{\int I(\lambda)d\lambda}}. \tag{2}$$

Figs. 3 and 4 show, respectively, the evolution of N_1 and of $N_2^{1/2}$ as the excitation wavelength changes, for all the doped fibers analyzed in this paper. It can be seen that PFO- and F8T2-doped fibers clearly yield the largest spectral changes when the excitation wavelength varies. Note that abrupt changes around the excitation wavelength of 400 nm are obtained in N_1 and $N_2^{1/2}$ for the PFO sample. In the case of the F8T2-doped fiber, the spectral changes are slightly smaller, and they are nearly unnoticeable in the other two doped fibers. The spectral changes observed in PFO- and F8T2-doped fibers suggest that

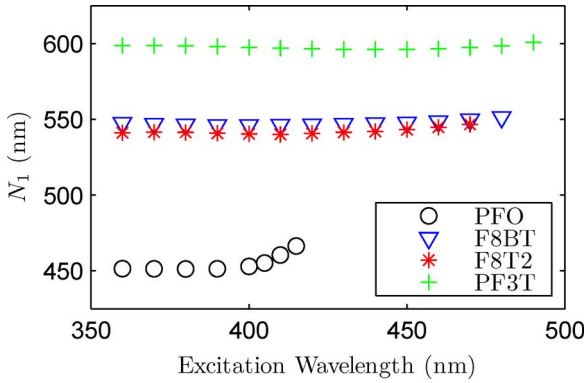

Fig. 3. Evolution of N_1 as a function of the excitation wavelength from POFs doped with PFO, F8BT, F8T2, and PF3T, and a light propagation distance of 16 cm. The excitation irradiance is 0.97 Wcm^{-2} in all cases.

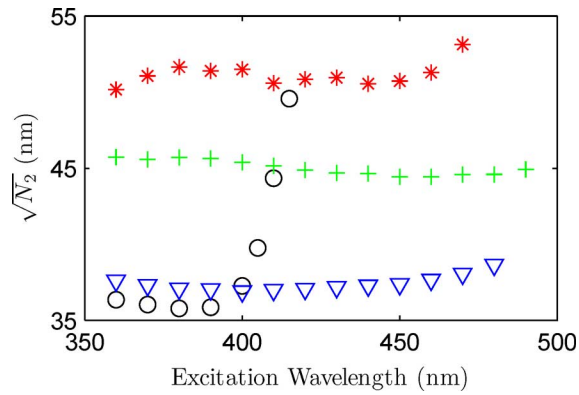

Fig. 4. Evolution of $N_2^{1/2}$ as a function of the excitation wavelength from POFs doped with PFO (o), F8BT (∇), F8T2 ($*$), and PF3T ($+$), and a light propagation distance of 16 cm. The excitation irradiance is 0.97 Wcm^{-2} in all cases.

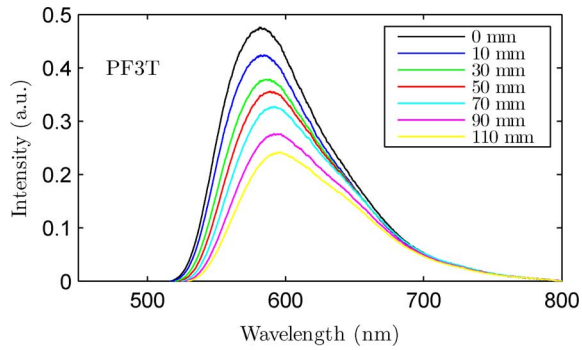

Fig. 5. Emission spectra as a function of light propagation distance for the PF3T-doped fiber exciting at 440 nm and with 0.97 Wcm^{-2} of irradiance. The point of the fiber closest to the detector has been normalized to zero.

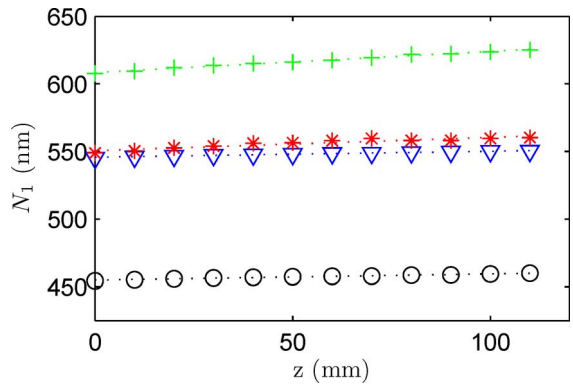

Fig. 6. Evolution of the first moments of the emission spectra as a function of the propagation distance exciting each fiber at the maximum-absorption wavelength and with 0.97 Wcm^{-2} of irradiance. The point of the fiber closest to the detector has been normalized to zero. The linear fittings are shown dotted. PFO (o); F8BT (∇); F8T2 ($*$); PF3T ($+$).

these dopants are dissolved inhomogenously during the manufacturing of the fibers. This hypothesis will be corroborated by AFM and TEM techniques in Section III-D.

B. Effect of the Propagation Distance on the Emission Spectra

The evolution of the emission spectra as a function of the light propagation distance z has been analyzed for all the doped fibers when exciting at the absorption maximum (see Table I). Fig. 5 shows the emission spectra obtained when the PF3T-doped fiber is excited at different launching points to vary the light propagation distance along the fiber. When the excitation point is moved farther from the detector, the amount of measured emitted intensity is reduced, and both the emission peak and the first moment are shifted toward longer wavelengths. It is known that these shifts are directly related to the overlap between the absorption and emission spectra [23]. This can be explained because the part of the emission situated in the emission-absorption overlap region is reabsorbed, and, in consequence, such short wavelengths of the overlap are more attenuated. Therefore, doped fibers with greater overlaps undergo higher red shifts in the first moment of their emission spectra when the propagation distance is increased. This fact is corroborated from our results plotted in Fig. 6, which shows the evolution of the first moments of the emission spectra as functions of the propagation distance. As can be seen, in all cases, there is a nearly linear red shift of the first moment, with different slopes depending on the dopant, when the light propagation distance is increased.

Table II shows the values of the slopes and of the coefficients of determination obtained from the linear fittings to each of the experimental curves of Fig. 6, as well as the absorption-emission overlaps. According to these data, it can be seen that the slope has a linear relationship with the overlap. The fact that shifts are experimentally found to be greater for greater overlaps corroborates the theoretical analysis shown in [23]. This is very important in order to know the tunable range of wavelengths in the design of POF lasers or amplifiers. Note, in Table II, that the coefficients of determination of the linear fittings are lower for the PFO- and F8T2-doped fibers, which could be related to the more inhomogeneous distribution of the dopant in the PMMA matrix.

Assuming that the illuminated fiber portion is a homogeneous light source (plane-wave source) and exciting with low irradiances, the output light measured at the fiber end at wavelength λ after propagating a distance z can be expressed by [16]

$$I(z,\lambda) = I_0(\lambda)\exp[-\alpha(\lambda)z]. \tag{3}$$

In (3), $I_0(\lambda)$ is the intensity spectrum at $z = 0$ and $\alpha(\lambda)$ is the linear attenuation coefficient. This expression fits properly for the range of wavelengths in the tail of the absorption spectrum of the dopant, i.e., close to or inside the overlap between

TABLE II
VALUES OF THE SLOPE OF THE EVOLUTION OF THE FIRST MOMENT AS A FUNCTION OF THE LIGHT PROPAGATION DISTANCE, OF THE COEFFICIENT OF DETERMINATION (R^2) OF THE LINEAR FITTING, AND OF THE OVERLAP BETWEEN THE ABSORPTION AND THE EMISSION SPECTRA, FOR EACH DOPED FIBER

	Slope (nm/mm)	R^2	Overlap (nm)
PFO	0.045	0.958	15
F8BT	0.044	0.984	15
F8T2	0.098	0.880	40
PF3T	0.156	0.990	80

the absorption and emission spectra. Out of this range, the expression does not fit properly due to reabsorption and reemission effects [24]. In order to clarify this idea, in Fig. 7, we plot the transmitted emission intensity as a function of the light propagation distance through each doped fiber at two different wavelengths. In all cases, one of the wavelengths was located inside the overlap region and the other one outside. At wavelengths located in the overlap region, the transmitted intensity follows an exponential behavior with a good fitting to (3), as can be seen in the coefficients of determination obtained. This means that the attenuation coefficients in that spectral range are constant along the length of the fiber. Out of that range, the transmitted intensity does not present the exponential behavior, because there is a reemission of the light absorbed at shorter wavelengths. The linear attenuation coefficients in the appropriate spectral ranges have been obtained by fitting the decays in the transmitted intensity with z to (3). These coefficients are shown in Fig. 8 for all the doped fibers analyzed.

C. Photostability

Let us now focus on the photostability of the doped fibers when they are illuminated with femtosecond laser pulses. We have observed that there was a clear reduction in the emission intensity with time when the doped fibers were excited under the conditions described in Section II. This reduction has been different for each doped fiber. Moreover, it has not been uniform spectrally, since we have observed a shift with exposure time in N_1 and in $N_2^{1/2}$ of the emission bands. In all of the measurements shown in previous sections, this fact was taken into account by recording each measurement after exposing the fiber until stabilization was achieved in the emitted spectrum.

In order to characterize the photostability of each doped fiber, first we have exposed the four doped fibers to the same excitation conditions for 60 min, with an excitation located at the wavelength of maximum absorption and with 0.97 Wcm^{-2} of irradiance. The results obtained for the photostability, for N_1 and for $N_2^{1/2}$ of the emitted spectrum, are shown in Fig. 9(a), (c), and (e). Fig. 9(b), (d), and (f) shows the evolution for 60 min of the same magnitudes under the same conditions, but after a rest interval in which the fibers were in darkness and at room temperature for 24 h. In the first measurements, the four doped fibers had never been exposed to laser light, so there was no previous degradation that could affect the results. In the second measurements, light was launched at exactly the same point of the fiber. For the sake of comparison, we have normalized the

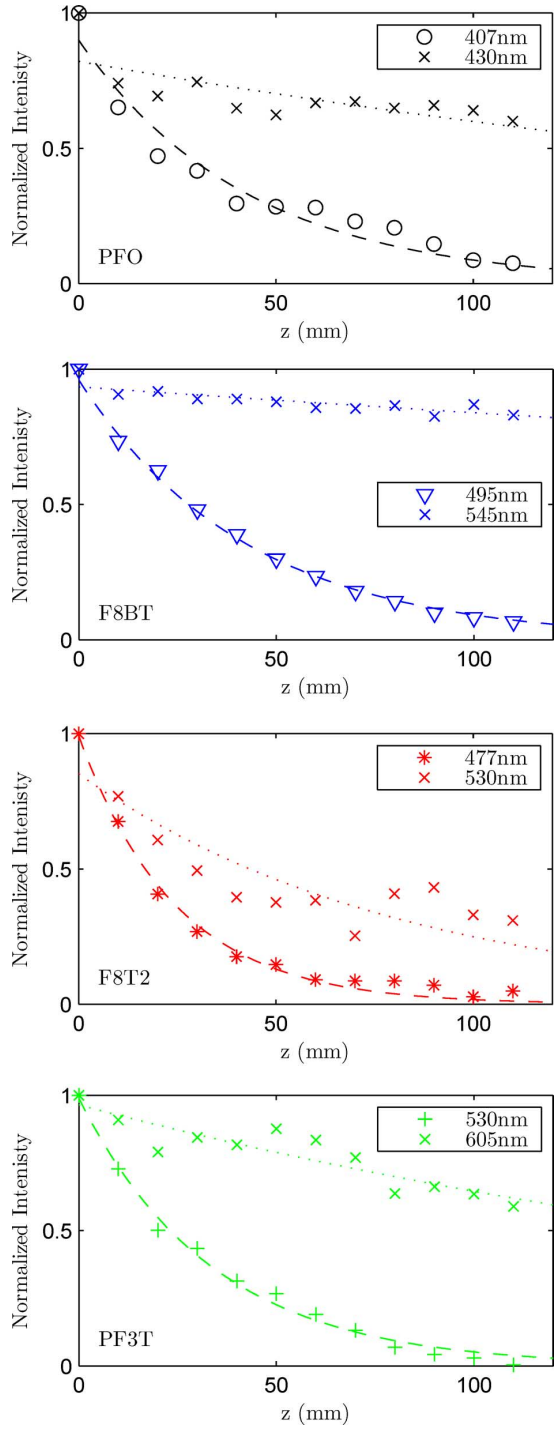

Fig. 7. Transmitted intensity as a function of z at different emission wavelengths, exciting at the maximum-absorption wavelength with 0.97 Wcm^{-2} of irradiance. The dashed and dotted lines are fittings using (3), with $R^2 = 0.9491$ (at 407 nm) and $R^2 = 0.5313$ (at 430 nm) for PFO, $R^2 = 0.9937$ (at 495 nm) and $R^2 = 0.6919$ (at 545 nm) for F8BT, $R^2 = 0.9906$ (at 477 nm) and $R^2 = 0.7739$ (at 530 nm) for F8T2, and $R^2 = 0.9920$ (at 530 nm) and $R^2 = 0.8175$ (at 605 nm) for PF3T-doped fibers.

fluorescence intensities to 100% at the start of the first measurements.

As can be noted in Fig. 9(a), F8BT- and PF3T-doped fibers are the most photostable ones. After 60 min of exposition at 80 MHz, which is equivalent to 2.88×10^{11} laser shots, the fluorescence capacities of both fibers are reduced by 25% and by

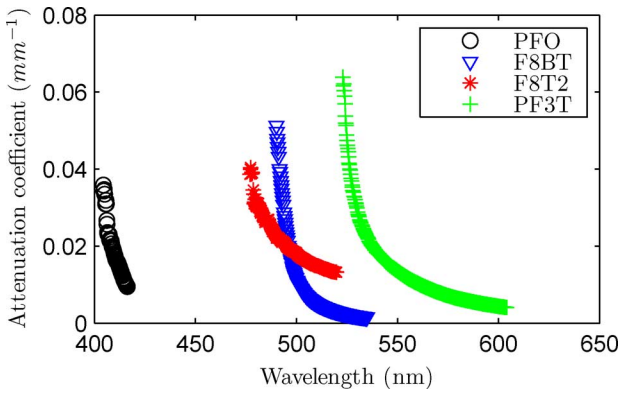

Fig. 8. Linear attenuation coefficients for all four doped fibers. The excitation wavelength in each case has been chosen at the maximum-absorption wavelength and with 0.97 Wcm^{-2} of irradiance.

45%, respectively. According to the definition of lifetime given in [25], which is the time elapsed before the fluorescence intensity is reduced by half, these two fibers have not reached their lifetime values yet. In the case of the other two doped fibers, i.e., F8T2 and PFO, their fluorescence capacities are affected much more, since they only maintain 9% of their initial intensities after the same period of time. On the other hand, their lifetimes are only of around 30 s (2.4×10^9 pulses) and 200 s (1.6×10^{10} pulses), respectively. In the case of PFO-doped fibers, part of this loss in the emission capacity can stem from the ultraviolet excitation wavelength, because high-energy photons contribute to reduce the photostability. By analyzing the decays of the emitted fluorescence shown in Fig. 9(a), we have seen that these can be well fitted to the following expression:

$$f(t) = a\exp(-t/\tau_1) + b\exp(-t/\tau_2) \tag{4}$$

in which a, b, τ_1, and τ_2 are constants. This type of intensity decay with two exponentials has also been reported in [26] and [27]. The values of these constants, obtained from the fittings, and the corresponding coefficients of determination are shown in Table III. In (4), the first exponential indicates how abruptly the emitted fluorescence decreases just at the beginning of the excitation period, whereas the second one stands for the decay in the long term. Therefore, larger values of τ_2 suggest that the slope with time in the relatively stable state is smaller, i.e., that the photostability is better. The values of τ_2 shown in Table III for F8BT- and PF3T-doped fibers corroborate that these are more stable samples than the other two ones in the long term.

Regarding the spectral changes with excitation time, Fig. 9(c) and (e) shows that the most noticeable ones also correspond to PFO- and F8T2-doped fibers. Specifically, there is a red shift in the first moments of 4 nm in the first 400 s in both cases, and there are spectral broadenings of 6 and 5 nm, respectively. Above this excitation time, there are not significant spectral changes. These spectral changes in the fluorescence with exposure time were also observed in rhodamine- or pyrromethene-doped POFs and related to the inhomogeneous distribution of the dopant in the matrix [11]. In the case of F8BT- and PF3T-doped fibers, we have not observed significant spectral changes in the evolution of the emission-capacity loss.

After 24 h of rest in darkness, there is a partial recovery in the fluorescence capacity only in the F8BT-doped fiber. Fig. 9(b) shows that the emission is initially 7% higher than at the last point of the first excitation period. This recovery could be due to the mechanism known as photoblinking [11], [27]. In such a process, the dopant molecules undergo transitions to a nonfluorescent or dark state, from which a few molecules are able to return to the initial state and recover the fluorescence capacity. In order to see if the recovery of the F8BT-doped fiber could be improved by increasing the period of rest, the sample was kept in darkness for another period of 42 h. Then, the sample was exposed again and we could see a 6% of recovery exciting at the same point of the fiber. This fact suggests that F8BT-doped fibers recover in 24 h nearly as much as in any longer time. We can also observe that the F8BT-doped fiber has not reached its lifetime value even at the end of the second excitation period. As for the spectral changes after 24 h of rest, it can be observed that the values of N_1 and $N_2^{1/2}$ of the emitted band do not practically change with respect to those obtained at the end of the first excitation period [see Fig. 9(d) and (f)].

Finally, we have analyzed spectroscopically the photostability of the F8BT-doped fiber as a function of the laser irradiance. The results obtained have been plotted in Fig. 10. It can be seen that, when the irradiance is increased, there is a slight displacement of the first moment towards longer wavelengths (red shift) and a small broadening of the spectral width. This behavior in the spectral width means that the employed irradiances are not high enough to obtain amplified spontaneous emission (ASE) [28], in which case a blue shift and a narrowing are expected. We have made our own computational simulations, similar to those reported in [29] and [30], in order to estimate what excitation irradiance is necessary to obtain ASE in F8BT-doped fibers under the same conditions (the same cladded step-index fiber with the same fiber length and dopant concentration). Our computational results have served us to conclude that the threshold irradiance (i.e., the minimum irradiance to achieve ASE) would be 1.22 MWcm^{-2} when using our ultrashort pulses (0.12 mJ/pulse) for this doped fiber. This theoretical threshold is of the same order as the experimental thresholds found in the literature for similar doped POFs [18], [31].

D. Dopant Distribution in PMMA POFs

In order to determine how the distribution of the dopant in PMMA POFs influences their spectroscopic characteristics and their photostability, we have obtained images of the four doped fibers using TEM and AFM techniques. In Fig. 11, which shows TEM images, the conjugated polymers appear as isolated black aggregates dispersed inside the PMMA matrix colored in light gray. As can be noted, PFO and F8T2 tend to link giving rise to bigger groups of aggregates and less homogenous dispersion. In contrast, F8BT and PF3T molecules are surrounded mainly by PMMA instead of being covered mainly by neighboring dopant molecules. Fig. 12 shows the corresponding AFM phase images for the same doped fibers. The differences in color indicate the existence of two different components and thus, clear phase separation. The bright areas correspond to each of the dopants, whereas the brownish areas represent the matrix

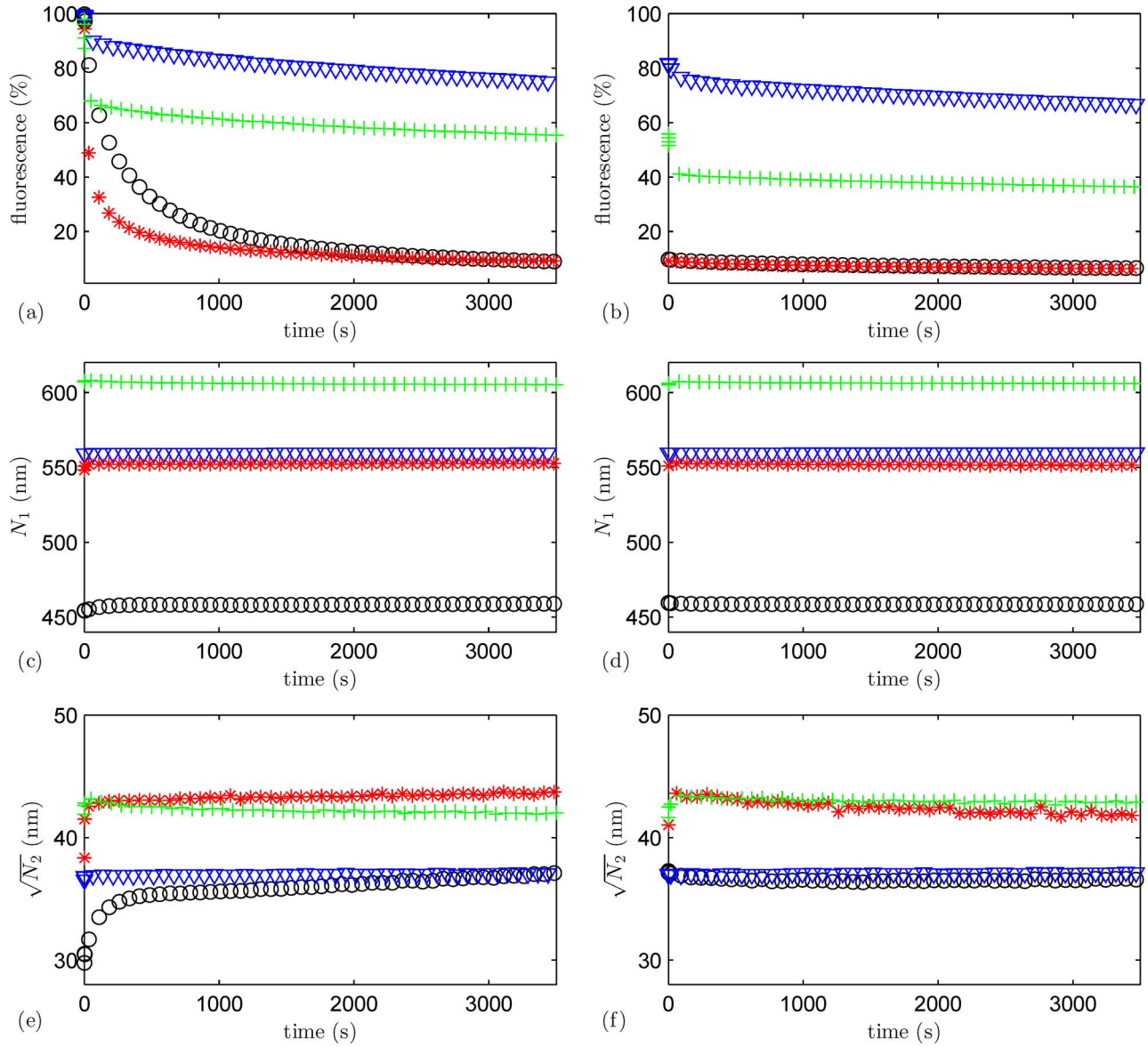

Fig. 9. Fluorescences, (a) and (b), first moments, (c) and (d), and square root of the second moments, (e) and (f), as functions of the excitation time. The excitation wavelengths are at the absorption maxima, the excitation irradiance is 0.97 Wcm^{-2}, and the light propagation distance is 16 cm. Fibers excited for up to 60 min in (a), (c), and (e). Fibers reexcited for another 60 min after a rest in (b), (d), and (f). PFO (o); F8BT (∇); F8T2 ($*$); PF3T ($+$).

TABLE III
VALUES OF THE FITTINGS TO THE EXPERIMENTAL CURVES OF FIG. 9(A) WITH (4)

	a	τ_1 (s)	b	τ_2 (s)	R^2
PFO	66,6	187,8	31,4	2366	0,996
F8BT	12,0	48,7	87,7	20934	0,993
F8T2	76,1	42,1	21,8	3147	0,990
PF3T	22,3	8,2	76,9	24450	0,993

formed by PMMA. The images of Fig. 12 confirm that only the molecules of PFO and of F8T2 form clear aggregations in the studied PMMA fibers. Both figures show clearly the different sizes of the aggregates, which reach even 1 μm of diameter in the case of the PFO-doped fiber. In the case of the F8T2-doped fiber, the dopant groups are smaller, being up to 500 nm of diameter. These images agree properly with the spectroscopic characteristics shown in this study. The nonuniform distribution of PFO and of F8T2 in the PMMA matrix can be related to their prominent spectral variations of the emission band and to the photostability characteristics already shown in this section.

The relationship between the photostability and the distribution of the dopant in the PMMA matrix can be explained from the rigidity of the solid matrix and the strength of its interaction with the molecules of dopant. Both properties reduce the probability of thermally excited reactions, which constitute the most common source of degradation in dye-doped polymers [32]. Moreover, it is known that those dye molecules directly surrounded by the PMMA matrix are partially isolated from reactive impurities [8], [25]. In consequence, the molecules of F8BT and PF3T surrounded by PMMA are partially protected from

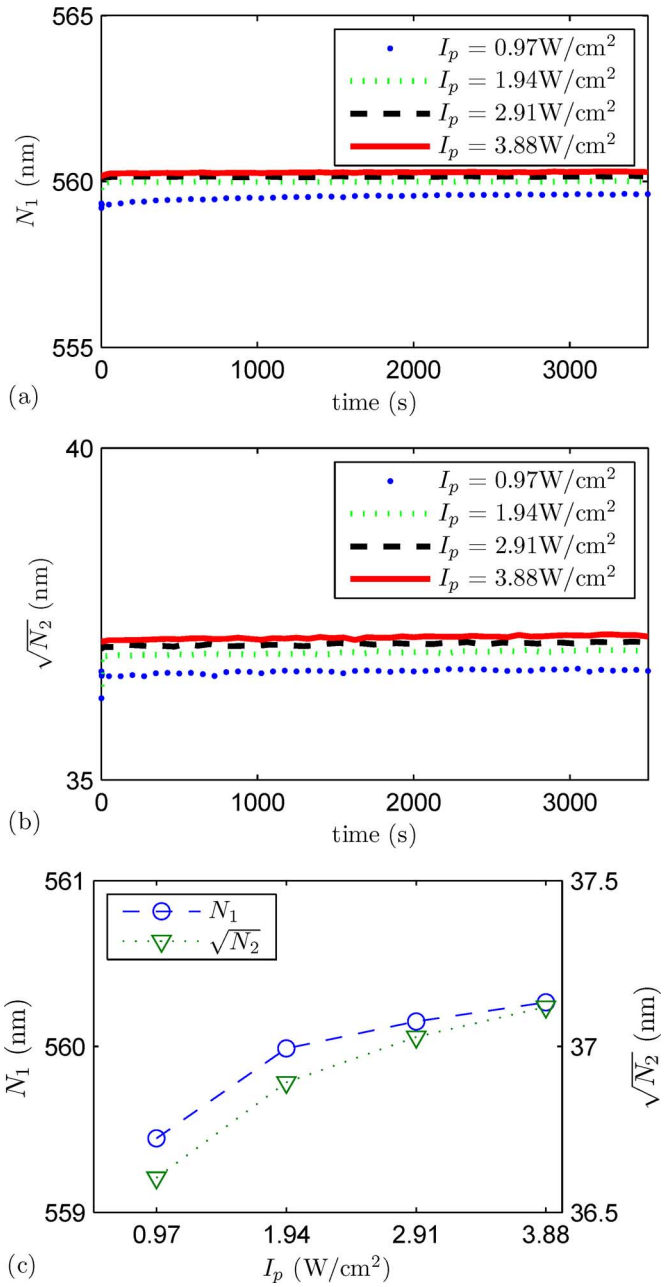

Fig. 10. Evolutions of the first moment (a) and of the square root of the second moment (b) as functions of the excitation time for the F8BT-doped fiber excited with four different irradiances at the maximum-absorption wavelength. Light propagation distance: 16 cm. (c) Dependence of both moments on the excitation irradiance at a fixed time of 500 s.

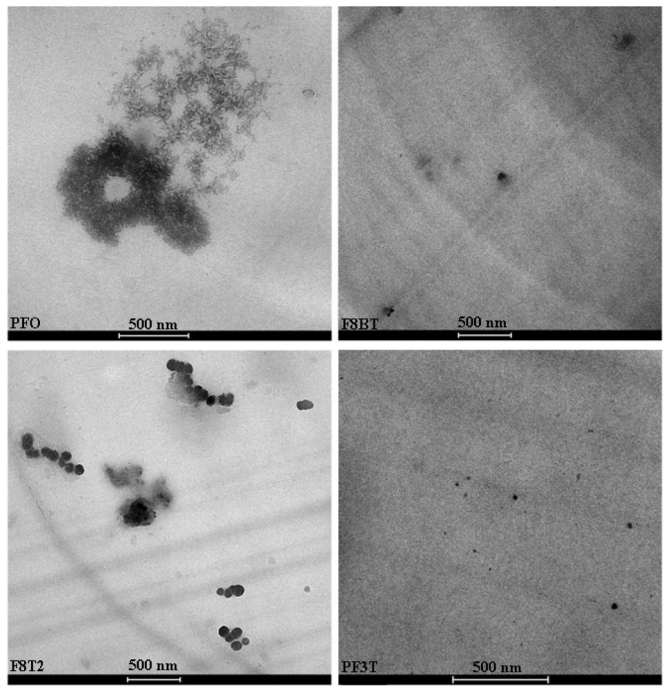

Fig. 11. TEM images of the four doped fibers. Conjugated polymer: in black. PMMA: in light gray.

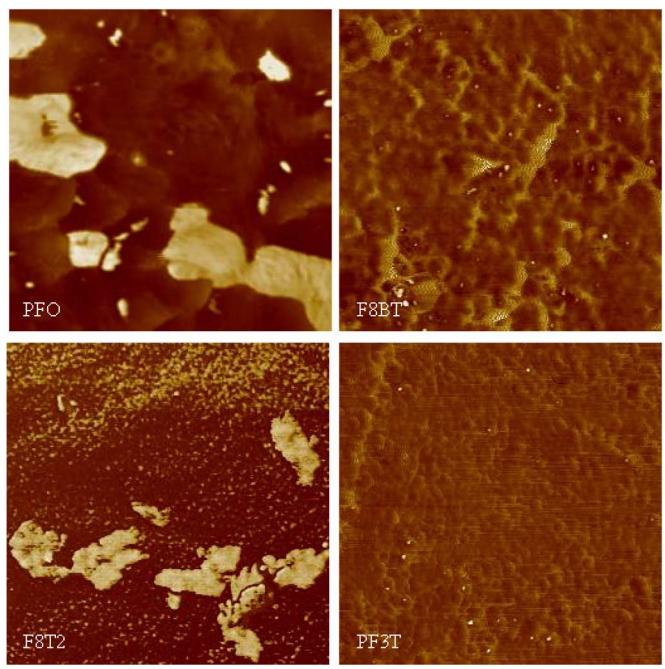

Fig. 12. AFM phase images of the four doped fibers. The area of the images is 1 μm $\times$ 1 μm in all cases. Brownish areas: PMMA. Bright areas: conjugated polymers.

the degradation effects, so the fibers conserve their emission capacity for a longer time. In contrast, the PFO- and F8T2-doped fibers, in which some of the molecules are not surrounded by the PMMA matrix, present a lower photostability. On the other hand, the fact that a more energetic excitation wavelength is used to excite the PFO-doped fiber may also contribute to reduce the photostability.

IV. Conclusion

The optical properties of four luminescent conjugated polymers embedded in POFs have been characterized by using a femtosecond laser. We have proved that the distribution of the dopant in the matrix has consequences both in the emission spectral characteristics and in the photostability. Those dopants prone to form aggregations in the fiber present greater variations in their emission spectral characteristics when the excitation wavelength changes, and their capacity to emit fluorescence intensity diminishes when they are excited with laser pulses for a sufficiently long period. F8BT-doped fibers present the highest photostability among the ones analyzed. We have also measured

the variations of the emission spectra as a function of the light propagation distance through the doped fibers. The longer the propagation distance, the more red-shifted the emission spectrum. The slope of the red shift is linearly related to the overlap between the absorption and the emission spectra. All these conclusions could also be true if different POF samples were taken from different POF manufacturers. The results analyzed in this paper are qualitatively valid if different PMMA POF samples are used, because optical behavior is mainly affected by the type of dopant, and only slightly by the surrounding medium. Therefore, this study can be very helpful for the design of optical lasers and amplifiers based on POF doped with conjugated polymers.

ACKNOWLEDGMENT

Technical and human support provided by SGIker (UPV/EHU, MICINN, GV/EJ, ERDF, and ESF) is gratefully acknowledged. The authors would also like to thank the collaboration of the engineer X. Azagirre.

REFERENCES

[1] J. Zubia and J. Arrue, "Plastic optical fibers: An introduction to their technological processes and applications," *Opt. Fiber Technol.: Mater., Devices Syst.*, vol. 7, no. 2, pp. 101–140, 2001.

[2] A. Tagaya, S. Teramoto, T. Yamamoto, K. Fujii, E. Nihei, Y. Koike, and K. Sasaki, "Theoretical and experimental investigation of rhodamine B-doped polymer optical fiber amplifiers," *IEEE J. Quantum Electron.*, vol. 31, no. 12, pp. 2215–2220, Dec. 1995.

[3] T. Kobayashi, K. Kuriki, N. Imai, T. Tamura, K. Sasaki, Y. Koike, and Y. Okamoto, "High-power polymer optical fiber lasers and amplifiers," *Proc. SPIE*, vol. 3623, pp. 206–214, 1999.

[4] A. Charas, A. L. Mendonça, J. Clark, G. Lanzani, L. Bazzana, A. Nocivelli, and J. Morgado, "Plastic optical fibers with gain and switching," in *Proc. Conf. Telecommun.*, 2009, pp. 121–124.

[5] A. Charas, A. L. Mendonça, J. Clark, J. Cabanillas-Gonzalez, L. Bazzana, A. Nocivelli, G. Lanzani, and J. Morgado, "Gain and ultrafast optical switching in PMMA optical fibers and films doped with luminescent conjugated polymers and oligomers," *Front. Optoelectron. China*, vol. 3, no. 1, pp. 45–53, 2010.

[6] A. Tagaya, S. Teramoto, E. Nihei, K. Sasaki, and Y. Koike, "High-power and high-gain organic dye-doped polymer optical fiber amplifiers: Novel techniques for preparation and spectral investigation," *Appl. Opt.*, vol. 36, no. 3, pp. 572–578, 1997.

[7] R. Xia, G. Heliotis, Y. Hou, and D. D. C. Bradley, "Fluorene-based conjugated polymer optical gain media," *Organ. Electron.*, vol. 4, no. 2–3, pp. 165–177, 2003.

[8] A. Dubonis, M. Canva, A. Brun, F. Chaput, and J. P. Boilot, "Photostability of dye molecules trapped in solid matrices," *Appl. Opt.*, vol. 35, pp. 3193–3199, 1996.

[9] I. Kaminow, L. Stulz, E. Chandross, and C. Pryde, "Photobleaching of organic laser dyes in solid matrices," *Appl. Opt.*, vol. 11, no. 7, pp. 1563–1567, 1972.

[10] Y. Nishizawa, S. Nishihara, K. Kuriki, A. Tagaya, and Y. Koike, "Lasing analysis of highly efficient rhodamine 6G-doped graded-index plastic optical fiber lasers," in *Proc. 16th Int. Plast. Opt. Fibers Conf.*, Torino, Italy, 2001, p. 105.

[11] G. D. Peng, Z. Xiong, and P. L. Chu, "Fluorescence decay and recovery in organic dye-doped polymer optical fibers," *J. Lightw. Technol.*, vol. 16, no. 12, pp. 2365–2372, Dec. 1998.

[12] U. Scherf, S. Riechel, U. Lemmer, and R. Mahrt, "Conjugated polymers: Lasing and stimulated emission," *Curr. Opin. Solid State Mater. Sci.*, vol. 5, no. 2–3, pp. 143–154, 2001.

[13] R. Palacios, P. Formentin, E. Martinez-Ferrero, J. Pallarès, and L. Marsal, "β-Phase morphology in ordered poly (9, 9-dioctylfluorene) nanopillars by template wetting method," *Nanoscale Res. Lett.*, vol. 6, no. 1, pp. 1–5, 2010.

[14] J. Jo, D. Vak, Y. Y. Noh, S. S. Kim, B. Lim, and D. Y. Kim, "Effect of photo- and thermo-oxidative degradation on the performance of hybrid photovoltaic cells with a fluorene-based copolymer and nanocrystalline TiO_2," *J. Mater. Chem.*, vol. 18, no. 6, pp. 654–659, 2008.

[15] A. Charas, J. Morgado, J. Martinho, L. Alcácer, and F. Cacialli, "Tuning the optoelectronic properties of polyfluorenes by copolymerisation with thiophene moieties," *Synth. Met.*, vol. 127, no. 1–3, pp. 251–254, 2002.

[16] R. Kruhlak and M. Kuzyk, "Side-illumination fluorescence spectroscopy. I. principles," *JOSA B*, vol. 16, no. 10, pp. 1749–1755, 1999.

[17] R. Kruhlak and M. Kuzyk, "Side-illumination fluorescence spectroscopy. II. Applications to squaraine-dye-doped polymer optical fibers," *JOSA B*, vol. 16, no. 10, pp. 1756–1767, 1999.

[18] M. Rajesh, M. Sheeba, K. Geetha, C. P. G. Vallaban, P. Radhakrishnan, and V. P. N. Nampoori, "Fabrication and characterization of dye-doped polymer optical fiber as a light amplifier," *Appl. Opt.*, vol. 46, no. 1, pp. 106–112, 2007.

[19] C. Pulido, "Multiple fluorescence sensing with side-pumped tapered polymer fiber," *Sens. Actuators B: Chem.*, vol. 157, pp. 560–564, 2011.

[20] L. Bazzana, G. Lanzani, R. Xia, J. Morgado, S. Schrader, and D. G. Lidzey, "Plastic optical fibers with embedded organic semiconductors for signal amplification," in *Proc. 16th Int. Plastic Opt. Fibers Conf.*, Torino, Italy, 2001, p. 327.

[21] M. G. Kuzyk, *Polymer Fiber Optics. Materials, Physics, and Applications*. New York: Taylor & Francis, 2007.

[22] B. P. Lyons, "Energy transfer to dopant molecules in polyfluorene films," Ph.D. dissertation, Dept. Phys., Univ. Durham, Durham, U.K., 2005.

[23] J. Arrue, F. Jimenez, M. A. Illarramendi, J. Zubia, I. Ayesta, I. Bikandi, and A. Berganza, "Computational analysis of the power spectral shifts and widths along dye-doped polymer optical fibers," *IEEE Photon. J.* vol. 2, no. 3, pp. 521–531, Jun. 2010.

[24] M. A. Illarramendi, J. Zubia, L. Bazzana, G. Durana, G. Aldabaldetreku, and J. R. Sarasua, "Spectroscopic characterization of plastic optical fibers doped with fluorene oligomers," *J. Lightw. Technol.* vol. 27, no. 15, pp. 3220–3226, Aug. 2009.

[25] M. Faloss, M. Canva, P. Georges, A. Brun, F. Chaput, and J. P. Boilot, "Toward millions of laser pulses with pyrromethene-and perylene-doped xerogels," *Appl. Opt.*, vol. 36, no. 27, pp. 6760–6763, 1997.

[26] A. Costela, F. Florido, I. Garcia-Moreno, R. Duchowicz, F. Amat-Guerri, J. Figuera, and R. Sastre, "Solid-state dye lasers based on copolymers of 2-hydroxyethyl methacrylate and methyl methacrylate doped with rhodamine 6G," *Appl. Phys. B*, vol. 60, no. 4, pp. 383–389, 1995.

[27] I. Rodrigues and J. Sanches, "Photoblinking/photobleaching differential equation model for intensity decay of fluorescence microscopy images," in *Proc. IEEE Int. Symp. Biomed. Imag.: Nano Macro*, 2010, pp. 1265–1268.

[28] I. D. W. Samuel, E. B. Namdas, and G. A. Turnbull, "How to recognize lasing," *Nature Photon.*, vol. 3, no. 10, pp. 546–549, 2009.

[29] I. Ayesta, J. Arrue, F. Jiménez, M. Illarramendi, and J. Zubia, "Computational analysis of the amplification features of active plastic optical fibers," *Phys. Status Solidi (a)*, vol. 208, no. 8, pp. 1845–1848, 2011.

[30] J. Arrue, F. Jiménez, I. Ayesta, M. A. Illarramendi, and J. Zubia, "Polymer-optical-fiber lasers and amplifiers doped with organic dyes," *Polymers*, vol. 3, no. 3, pp. 1162–1180, 2011.

[31] T. Kobayashi and W. Blau, "Laser emission from conjugated polymer in fibre waveguide structure," *Electron. Lett.*, vol. 38, no. 2, pp. 67–68, 2002.

[32] G. D. Peng, P. Chu, Z. Xiong, T. W. Whitbread, and R. P. Chaplin, "Dye-doped step-index polymer optical fiber for broadband optical amplification," *J. Lightw. Technol.*, vol. 14, no. 10, pp. 2215–2223, Oct. 1996.

Author biographies not included by author request due to space constraints.